PROCEEDINGS OF SCIENCE

GRB afterglow emission models with mixed electron distributions

Ioulia Florou* **and Maria Petropoulou***

**National and Kapodistrian University of Athens,*
Zografos, GR 15783, Greece

E-mail: iflorou@phys.uoa.gr, mpetropo@phys.uoa.gr

Gamma-ray bursts (GRBs) are intense and short flashes of γ-rays followed by the afterglow, which is a long lasting multi-wavelength emission. Very-high-energy (VHE, $E > 100$ GeV) photons have been recently detected from a couple of GRBs during the afterglow. In this contribution, we numerically investigate the production of VHE photons in GRB afterglows in the context of a leptonic synchrotron self-Compton model. We study the impact of a mixed accelerated electron distribution that is composed of non-thermal (power law) and thermal (Maxwell–Jüttner) components on the gamma-ray afterglow spectra and light curves. When the thermal electron distribution carries most of the total particle energy, the light curves in specific energy ranges may deviate from the standard power-law decay, and the γ-ray spectra may show multiple spectral components attributed to the synchro-Compton process of thermal and non-thermal electrons.

7th Heidelberg International Symposium on High-Energy Gamma-ray Astronomy (Gamma2022)
4-8 July 2022
Barcelona, Spain

PoS(Gamma2022)194

1. Introduction

Gamma-ray bursts (GRBs) are the most luminous explosions in the universe. The prompt GRB phase, which is characterised by the emission of brief but intense flashes of γ-rays, is followed by the afterglow, i.e., a long-lasting emission spanning a wide range of energies, from radio waves to γ-rays. While the origin of the prompt emission is still debated, there is a satisfactory explanation for the production of the bulk of the afterglow radiation. The broadband long-living emission of GRB afterglows suggests the presence of relativistic particles with extended, power-law like energy distributions. The part of the afterglow emission detected in the radio, optical, X-rays, and sub-GeV energy bands is described reasonably well by the synchrotron emission of relativistic electrons accelerated in a relativistic blast wave (RBW) that propagates in the circumburst medium [12]. Additionally, the same electrons that radiate synchrotron can inverse-Compton scatter synchrotron photons to higher energies [3, 10]. The interest in the so-called synchrotron self-Compton (SSC) model for γ-ray production has regained attention after the recent detection of afterglows in TeV energies by MAGIC and H.E.S.S. [5, 7].

Particle acceleration at relativistic shocks has been extensively studied as a potential mechanism to energise particles into power-law distributions [13]. Particle-in-cell (PIC) simulations of plasma processes study from first principles the interaction of particles with their own generated electromagnetic fields. Such simulations show that the majority of the upstream electrons picked up by the shock isotropise in the downstream region, and thermalise at a characteristic temperature $\Theta \sim \Gamma/3$ (in units of $m_e c^2$) for electron-positron ($e^- e^+$) plasmas, where Γ is the RBW bulk Lorentz factor. The *thermal* component can be well described by a relativistic Maxwell–Jüttner distribution. The *non-thermal* electron component, carrying a fraction η of the total available energy, typically emerges at Lorentz factors a few times larger than Θ, having a power-law distribution. Motivated by these findings, [4] assumed a mixed thermal and non-thermal electron distribution and studied the emitted synchrotron spectra and light curves for $\eta < 1$. One of their findings was that the X-ray afterglow spectra show a characteristic hard $\longrightarrow$ soft $\longrightarrow$ hard evolution. Recently, [15] studied the SSC emission from mixed electron distributions, focusing on cases with $\eta \sim 1$.

In this work we adopt the mixed thermal/power-law electron distribution and numerically compute multi-wavelength photon spectra and light curves in the context of an SSC model for $0.01 \leq \eta \leq 1$, paying special attention to the GeV-to-TeV emission. We limit our discussions to a constant-density circumburst medium and a specific set of RBW parameters. A more extensive study of the parameter space, including a wind-like density profile, will be presented in *Florou et al. (in prep.)*. We do not account for the existence of a reverse shock, which may contribute to the early afterglow emission, or the lateral spreading of the ejecta, which may become relevant at late times. We adopt $z = 0.4$ as a typical redshift for VHE-detected GRB afterglows and use $H_0 = 69.32$ km Mpc^{-1} s^{-1}, $\Omega_{\rm M} = 0.29$, $\Omega_\Lambda = 0.71$ [6].

2. Model

We assume a spherical adiabatic RBW with energy E that starts propagating from an initial radius $R_{\rm in}$ with bulk Lorentz factor $\Gamma_{\rm in} \gg 1$ in a circumburst medium of mass density $\rho_{\rm ext}$. The bulk kinetic energy of the outflow is converted to internal energy, part of which is radiated away by

relativistic particles. The evolution of the total mass of the RBW M and its Lorentz factor Γ with radius R are governed by [2]:

$$\frac{d\Gamma}{dR} = -\frac{4\pi R^2 \rho_{\rm ext}(\Gamma^2-1)}{M}, \quad \frac{dM}{dR} = 4\pi R^2 \rho_{\rm ext}\Gamma, \tag{1}$$

where $R = R_{\rm in} + \beta_\Gamma c(t - t_{\rm in})$ and $\beta_\Gamma \sim 1$ as long as the blast wave remains relativistic. t is measured in the central engine frame and is related to the comoving time t' as $t \sim \int dt'/(2\Gamma)$. The time in the observer's frame is then $t_{\rm obs} = (1+z)t$. The RBW starts decelerating when the swept-up mass, $M_{\rm sw} = (4/3)\pi R^3 \rho_{\rm ext}$, equals the initial mass $M_{\rm in} = E/\Gamma_{\rm in} c^2$, i.e., $\Gamma \propto R^{-3/2}$ for $R > \left(3E/(4\pi\rho_{\rm ext}c^2)\right)^{1/3}$.

We consider the downstream region of the shock as the radiation zone where particles are injected with a mixed thermal and non-thermal distribution. Electrons pick up a fraction $\epsilon_{\rm e}$ of the accreted kinetic energy,

$$\epsilon_{\rm e}\frac{dE}{dt} = \epsilon_{\rm e} 4\pi R^2 \rho_{\rm ext} c^3 \beta_\Gamma \Gamma(\Gamma-1) = m_{\rm e}c^2 V \int_1^\infty d\gamma\,(\gamma-1)\,Q_{\rm e}^{\rm (inj)}(\gamma), \tag{2}$$

where $m_{\rm e}$ is the electron rest mass, $V = 4\pi R^2 r$ is the volume of a spherical shell with comoving width $r = R/\Gamma$, and $Q_{\rm e}^{\rm (inj)}(\gamma)$ is the volumetric particle injection rate. A fraction $(1-\eta)$ of the total electron luminosity is injected into a Maxwell–Jüttner distribution, while the remaining fraction η goes into a power-law component with slope p starting from $\gamma_{\rm nth}$ [4]:

$$Q_{\rm e}^{\rm (inj)}(\gamma) = \frac{dN_{\rm e}}{d\gamma dt dV} = \frac{C}{2\Theta^3}\begin{cases} \gamma^2 e^{-\gamma/\Theta}, & \text{if } \gamma \le \gamma_{\rm nth} \\ \gamma_{\rm nth}^2 e^{-\gamma_{\rm nth}/\Theta}\left(\frac{\gamma}{\gamma_{\rm nth}}\right)^{-p}, & \text{if } \gamma > \gamma_{\rm nth}. \end{cases} \tag{3}$$

Here C is a normalisation constant determined by Eq. 2, $\Theta \approx \epsilon_{\rm e}(1-\eta)(m_{\rm p}/m_{\rm e})(\Gamma/3)$ and $\gamma_{\rm nth} = 3\Theta$ for $\eta < 1$, or $\epsilon_{\rm e}(p-2)/(p-1)(m_{\rm p}/m_{\rm e})\Gamma$ for a pure power law ($\eta = 1$), with $m_{\rm p}$ being the proton rest mass. The power law is terminated at a maximum Lorentz factor that is typically limited by synchrotron cooling at $\gamma_{\rm max} \gg \gamma_{\rm nth}$ [see, e.g., Eq. (26) in 14]. For simplicity, we adopt a constant value of $\gamma_{\rm max} = 10^{7.3}$.

Relativistic electrons that are injected into the downstream region will emit synchrotron radiation in the local magnetic fields. Assuming that the magnetic energy density is a fraction $\epsilon_{\rm B}$ of the internal energy density in the downstream region, one can derive the magnetic field strength in the shocked fluid frame:

$$B = \Gamma\sqrt{32\pi\epsilon_{\rm B}\rho_{\rm ext}c^2}. \tag{4}$$

3. Numerical Approach

We use a numerical code, similar to the one described in [8], that solves two coupled integro-differential equations for electrons and photons inside an expanding spherical volume of instantaneous radius r:

$$\frac{\partial n_{\rm e}}{\partial t} + c\frac{3n_{\rm e}}{r} = Q_{\rm e} + \mathcal{L}_{\rm e} \tag{5}$$

$$\frac{\partial n_\gamma}{\partial t} + c\frac{3n_\gamma}{r} + \frac{n_\gamma}{t_{\gamma,\rm esc}} = Q_\gamma + \mathcal{L}_\gamma \tag{6}$$

The above equations describe the evolution of the electron and photon differential number densities, $n_{\rm e}$ and n_γ, respectively. We assume that the electrons are confined in the blob ($t_{\rm esc,e} \to \infty$) and only photons escape on a timescale $t_{\rm esc,\gamma} = r/c$. The operators for losses ($\mathcal{L}_{\rm e,\gamma}$) and injection ($Q_{\rm e,\gamma}$) include the following processes: synchrotron radiation, synchrotron self-absorption, IC scattering, photon-photon pair production and adiabatic losses. All quantities that depend on Γ are updated at every time step by solving Eq. (1) and evaluating Eq. (2).

4. Results & Conclusions

We investigate the role of the parameter η in the resulting photon spectra and light curves. We present results for three indicative values, starting with $\eta = 1$ (i.e., pure power-law injection), and progressively decreasing the amount of energy injected into the power law, with $\eta = 0.1$ and 0.01. In all cases, we assume a GRB fireball with total energy $E = 10^{53}$ erg at the onset of the afterglow, $R_{\rm in} = 10^{13}$ cm, and $\Gamma_{\rm in} = 400$. The number density of the circumburst medium is $n = 1$ cm^{-3}. The power-law slope is fixed to $p = 2.3$ and the energy fractions for the electrons and magnetic field are $\epsilon_{\rm e} = 0.3$ and $\epsilon_{\rm B} = 0.003$, respectively. We end the simulations when the RBW radius becomes $6000\, R_{\rm in}$.

The resulting broadband photon spectra are depicted in Fig. 1, where we indicate with colour the temporal evolution. There is a strong dependence of the broadband photon spectra on η. For instance, for $\eta = 0.1$ one can clearly identify (especially at later times) the synchrotron components of the thermal and power-law electron distributions as well as the synchro-Compton component of the thermalised electrons. At any given time, the synchrotron emission of the power-law electrons bridges the low-energy and high-energy components of the spectrum that are related to the Maxwellian electron distribution. For $\eta = 0.01$, the overall emission is dominated by the thermalised electron population, thus resulting in considerably narrower low- and high-energy spectral components than the typical case of $\eta = 1$.

In the left panel of Fig. 2 we present the keV, GeV, and TeV light curves, computed for $\eta = 1$ and 0.1 (solid and dashed lines, respectively). The X-ray and TeV light curves for $\eta = 0.1$ show a steepening at a few thousand seconds, when the synchrotron and synchro-Compton peaks of the thermal electron component cross the respective energy range; this behaviour agrees with the results of [4] about the synchrotron X-ray afterglow light curves. Another interesting finding is that the 0.1-1 GeV light curves show a shallow decline, which becomes more prominent with the decrease in η. This shallower flux decay is expected when the $F(\epsilon) \propto \epsilon^{1/3}$ tail of the synchro-Compton spectrum of the Maxwellian electron distribution crosses the specific energy band. During this time window the spectrum also hardens [see also 9]. A comparison of the γ-ray spectra for $\eta = 1$ and 0.1 at three indicative times can be seen in the right panel of the same figure. Note the differences in the spectral slope in the 0.1-1 GeV range between $\eta = 1$ and 0.1 at these three instances.

In general, shock acceleration produces a mixed thermal (Maxwell-Jüttner) and a non-thermal (power law) electron distribution. The amount of energy carried by the thermal component is imprinted on the broadband afterglow spectra and narrow-band light curves. For example, when the thermal electron component carries more than 50% of the total particle energy, a shallow decay

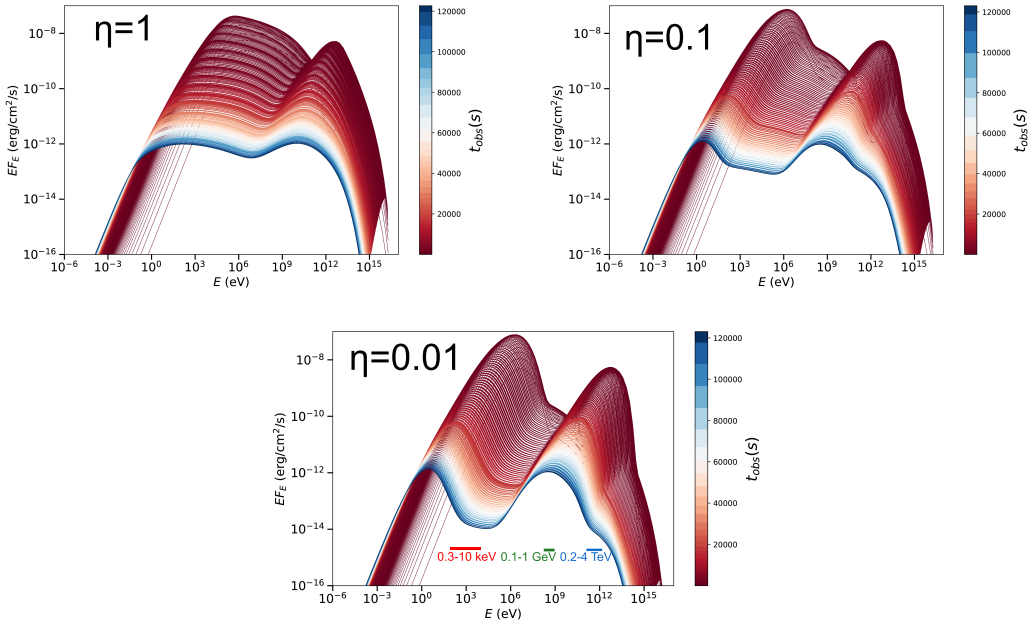

Figure 1: Temporal evolution of the afterglow broadband photon spectra for three choices of the energy fraction injected into the power-law electron distribution, i.e., $\eta = 1$, 0.1, and 0.01. The Extragalactic Background Light (EBL) absorption is not taken into account.

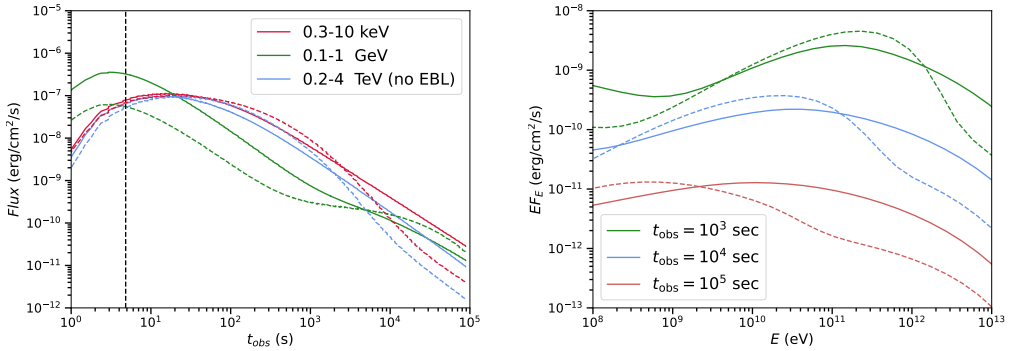

Figure 2: *Left panel:* X-ray, GeV and TeV afterglow light curves computed for $\eta = 1$ (solid lines) and 0.1 (dashed lines). All other parameters are the same as in Fig. 1. The vertical black dashed line corresponds to the moment the RBW deceleration is initiated. *Right panel:* Snapshots focusing on the γ-ray part of the spectrum for $\eta = 1$ (solid lines) and 0.1 (dashed lines) for the times 10^3, 10^4, 10^5 sec which are colour coded.

of the GeV light curves is predicted. This result can be then confronted with light curves of GRBs detected by *Fermi*-LAT [1] in order to constrain the thermal electron population in GRB afterglows (*Florou et al. in prep*).

5. Acknowledgements

The authors acknowledge support from the MERAC Fondation through project THRILL.

References

[1] Ajello M., Arimoto M., Axelsson M., Baldini L., Barbiellini G., Bastieri D., Bellazzini R., et al., 2019, ApJ, 878, 52. *A Decade of Gamma-Ray Bursts Observed by Fermi-LAT: The Second GRB Catalog*

[2] Blandford R. D., McKee C. F., 1976, PhFl, 19, 1130.*Fluid dynamics of relativistic blast waves*

[3] Chiang J., Dermer C. D., 1999, ApJ, 512, 699. *Synchrotron and Synchrotron Self-Compton Emission and the Blast-Wave Model of Gamma-Ray Bursts*

[4] Giannios D., Spitkovsky A., 2009, MNRAS, 400, 330. *Signatures of a Maxwellian component in shock-accelerated electrons in GRBs*

[5] H. E. S. S. Collaboration, Abdalla H., Aharonian F., Ait Benkhali F., Angüner E. O., Arcaro C., Armand C., et al., 2021, Sci, 372. *Revealing x-ray and gamma ray temporal and spectral similarities in the GRB 190829A afterglow*

[6] Hinshaw G., Larson D., Komatsu E., Spergel D. N., Bennett C. L., Dunkley J., Nolta M. R., et al., 2013, ApJS, 208, 19. *Nine-year Wilkinson Microwave Anisotropy Probe (WMAP) Observations*

[7] MAGIC Collaboration, Acciari V. A., Ansoldi S., Antonelli L. A., Engels A. A., Baack D., Babić A., et al., 2019, Natur, 575, 459. *Observation of inverse Compton emission from a long γ-ray burst*

[8] Petropoulou M., Mastichiadis A., 2009, A&A, 507, 599. *On the multiwavelength emission from gamma ray burst afterglows*

[9] Petropoulou M., Mastichiadis A., Piran T., 2011, A&A, 531, A76. *Effects of a low electron distribution cutoff on multiwavelength spectra and light curves of GRB afterglows*

[10] Sari R., Esin A. A., 2001, ApJ, 548, 787. *On The Synchrotron Self-Compton Emission from Relativistic Shocks and Its Implications for Gamma-Ray Burst Afterglows*

[11] Sari R., Narayan R., Piran T., 1996, ApJ, 473, 204. *Cooling Timescales and Temporal Structure of Gamma-Ray Bursts*

[12] Sari R., Piran T., Narayan R., 1998, ApJL, 497, L17. *Spectra and Light Curves of Gamma-Ray Burst Afterglows*

[13] Sironi L., Keshet U., Lemoine M., 2015, SSRv, 191, 519. *Relativistic Shocks: Particle Acceleration and Magnetization*

[14] Sironi L., Spitkovsky A., Arons J., 2013, ApJ, 771, 54. *The maximum energy of accelerated particles in relativistic collisionless shocks*

[15] Warren D. C., Dainotti M., Barkov M. V., Ahlgren B., Ito H., Nagataki S., 2022, ApJ, 924, 40. *A Semianalytic Afterglow with Thermal Electrons and Synchrotron Self-Compton Emission*